

Wave propagation across interfaces between two Hertz-like granular crystals with different interaction exponents

Armin Kekić and Robert A. Van Gorder*
*Mathematical Institute, University of Oxford,
 Andrew Wiles Building,
 Radcliffe Observatory Quarter, Woodstock Road,
 Oxford, OX2 6GG, United Kingdom*
 *Robert.VanGorder@maths.ox.ac.uk

We study solitary wave propagation in 1D granular crystals with Hertz-like interaction potentials. We consider interfaces between media with different exponents in the interaction potential. For an interface with increasing interaction potential exponent along the propagation direction we obtain mainly transmission with delayed secondary transmitted and reflected pulses. For interfaces with decreasing interaction potential exponent we observe both significant reflection and transmission of the solitary wave, where the transmitted part of the wave forms a multipulse structure. We also investigate impurities consisting of beads with different interaction exponents compared to the media they are embedded in, and we find that the impurities cause both reflection and transmission, including the formation of multipulse structures, independent of whether the exponent in the impurities is smaller than in the surrounding media. We explain wave propagation effects at interfaces and impurities in terms of quasi-particle collisions.

I. INTRODUCTION

Granular materials are composed of a large number of discrete, solid macroscopic particles such as sand, rice or snow; and they play an important role in many aspects of industry and science such as construction, agriculture or geological processes. They are often viewed as a fourth state of matter as they can exhibit characteristics of gases, liquids or solids, depending on the circumstances [1]. One of the most exciting features of granular crystals we want to study is the wave propagation. Compression waves can propagate as solitons or sound waves depending on the interaction potential between the beads and the external compression of the chain. In uniform granular crystals solitons can travel over distances that are orders of magnitude larger than the wavelength without experiencing any change in shape due to dispersion [2]. The type of interaction that leads to non-linear solitary waves is the repulsive Hertz-like contact force that depends on the contact geometry and bead material [3]. Even though solitary waves are stable in uniform granular chains [2], they can undergo drastic changes at interfaces between media with different properties [4]. The wave can be partially transmitted or reflected, and even the full disintegration of the wave into so-called multipulse structures is observed [5, 6]. While most of the work done on interfaces so far focuses on media with different bead masses, we use differences in the contact geometry between the beads as an alternative approach to tweak the wave propagation dynamics at interfaces. The shape of the interaction potential depends on the geometry of the contact region, which in turn affects the wave propagation [4].

The interesting wave propagation properties in granular crystals, as depicted in Fig. 1, originate in the interaction between neighbouring beads in the chain. Two elastic bodies in contact experience a repulsive force which

depends on the compression. Considering two bodies i and $i+1$ at positions x_i and x_{i+1} , the repulsive force can be obtained by the interaction potential

$$V(\delta_{i,i+1}) = a_{i,i+1} \delta_{i,i+1}^{n_{i,i+1}}, \quad (1)$$

where $\delta_{i,i+1}$ is the virtual overlap between the two bodies presuming they would not deform, and $a_{i,i+1}$ is a prefactor depending on the elastic properties of the material and the geometry of the contact region [3, 7]. We assume that the mutual force between beads is given only by contact forces and therefore $V \equiv 0$ for $\delta_{i,i+1} = 0$, i.e. there is no long-range interaction. The value of the exponent $n_{i,i+1}$ is determined by the contact region geometry [3, 4].

The repulsive force between beads is related to the interaction potential by

$$F(\delta) = -\frac{\partial}{\partial \delta} V(\delta). \quad (2)$$

We only consider interactions with $n_{i,i+1} > 2$, for which the forces between the beads are non-linear in δ . This leads to the formation of non-linear waves, for which the propagation speed depends on the amplitude. Furthermore, we note that the inter-particle force originating from the potential (1) is fully non-linear, i.e. the force has no linear component. As a direct consequence of that, sound wave propagation is not possible in granular crystals without external precompression [2]. Such media are sometimes referred to as *sonic vacua* [2].

For spheres with radii R_i and R_{i+1} the exponent is $n_{i,i+1} = 5/2$ and the prefactor is given by

$$V(\delta_{i,i+1}) \stackrel{\text{spheres}}{=} \frac{2}{5D_{i,i+1}} \sqrt{\frac{R_i R_{i+1}}{R_i + R_{i+1}}} \delta_{i,i+1}^{5/2}, \quad (3)$$

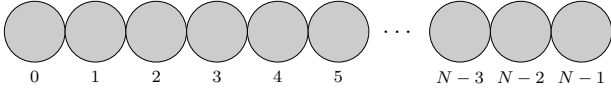


Figure 1: Granular chain composed of uniform media. Note that in the experimental implementation the beads are not spherical in general.

$$D_{i,i+1} = \frac{3}{4} \left[\frac{1 - \sigma_i^2}{Y_i} + \frac{1 - \sigma_{i+1}^2}{Y_{i+1}} \right], \quad (4)$$

where the Young moduli Y_i, Y_{i+1} and the Poisson ratios σ_i, σ_{i+1} are determined by the elastic properties of the bead materials. Equation (3) is called *Hertz potential* [8, 9]; systems with the more general interaction potential (1) are sometimes called *Hertz-like*.

The overlap for spherical beads is given by

$$\delta_{i,i+1} = ((R_i + R_{i+1}) - x_{i+1} + x_i)_+, \quad (5)$$

with $v_+ := \max(v, 0)$. It is often more convenient to write the overlap in terms of the displacements rather than the absolute positions of the beads. For bead i the displacement is $u_i = x_i - x_{i,0}$, where $x_{i,0}$ is the initial position, and the overlap becomes

$$\delta_{i,i+1} = (\Delta_{i,i+1} - u_{i+1} + u_i)_+. \quad (6)$$

The precompression $\Delta_{i,i+1}$ accounts for the fact that the initial position of the beads need not be such that the beads are barely touching, i.e. touching but not overlapping. They can also be precompressed by squeezing the chain from both ends.

The potential (1) is, strictly speaking, a result for the static case, i.e. Equation (1) relates the overlap between the beads to an externally applied static force. This result only remains valid for the dynamic case if the time scale of the change in force is much larger than the time that a longitudinal acoustic wave would need to travel across the length of the bead [10]. This restriction ensures that the internal dynamics of the bead can be neglected for the study of the dynamics in the chain. We use similar chain parameters as in the experimental study carried out by Coste et al. [10] in order ensure the validity of this approximation. Therefore, we can treat the beads as point-like masses that interact via (1).

A noteworthy property of the type of granular chains we want to study is that they can be torn apart without any resistance, which is a consequence of the fact that there is no long-range interaction between the beads. This is sometimes referred to as the chain having *zero tensile strength*. Therefore, gaps can open between beads in the chain; and without external compression these can only be closed by interacting with other beads.

From Equation (1) one can derive Newton's equation of motion for the i^{th} bead, with $i \in \{0, \dots, N-1\}$, in a

granular chain

$$\begin{aligned} \frac{d^2 u_i(t)}{dt^2} = & \frac{1}{m_i} \underbrace{W_i}_{\text{external field}} \\ & + \frac{n_{i-1,i} a_{i-1,i}}{m_i} \underbrace{(\Delta_{i-1,i} + u_{i-1}(t) - u_i(t))_+^{n_{i-1,i}-1}}_{\text{left neighbour}} \\ & - \frac{n_{i,i+1} a_{i,i+1}}{m_i} \underbrace{(\Delta_{i,i+1} + u_i(t) - u_{i+1}(t))_+^{n_{i,i+1}-1}}_{\text{right neighbour}}. \end{aligned} \quad (7)$$

Here, the first two terms describe the interaction with the left and right neighbour respectively. In addition to the mutual repulsive contact force described by Equation (1), an external force field, such as gravity, can be applied to the beads, which is accounted for in the last term. For the beads at the end of the chain the relevant neighbour interaction term needs to be set to zero. Chains in which all the beads and precompressions are equal are called *monodisperse*, and *polydisperse* otherwise. We call a bead *excited* if it has significant overlap with at least one of its neighbours; in other words, if there is some potential energy stored in the interaction with a neighbouring bead.

The existence of solitary waves in granular chains was first theoretically predicted using a continuum model by Nesterenko [11] and experimentally verified by Lazard and Nesterenko [12] and later by Coste et al. [10]. The analytical formulation for the propagation of a single solitary wave through a granular crystal under the assumption of a continuous medium [2, 4] shows good agreement with experiments and numerical simulations for simple solitary wave propagation in monodisperse media [10, 12, 13]. However, in more complex situations the discreteness of granular media can play an essential role for the wave propagation behaviour. For example, in the case of two colliding solitary waves the analytical description predicts that the two waves pass each other without changing their shape and amplitude, whereas numerical simulations of the discrete medium suggest the emergence of secondary solitary waves from the collision [4, 14, 15].

The simplest form of a polydisperse chain is one which consists of two jointed monodisperse granular chains with different bead masses. The behaviour of a solitary wave propagating across the interface between the two media depends on the side from which the wave initially approaches the interface. In numerical investigations, the partial transmission and reflection of the incoming wave are observed for a solitary wave propagating across an interface from a medium with light grains to one with heavier grains [4–6]. Furthermore, during the splitting of the incoming wave into a transmitted and a reflected part, gaps arise between beads at the vicinity of the interface [6]. Similar effects to those at interfaces between granular crystals with different bead masses have been

observed for mass impurities. These impurities are created by changing the mass of a single bead in an otherwise monodisperse granular crystal [4, 13, 16]. For a wave travelling in the opposite direction of the jointed chain, the incoming wave is fully transmitted and disintegrates forming a multipulse structure [6, 17]. A second multipulse structure is formed with a delay to the first one. This delay is due to a gap opening and closing between beads at the interface.

Wave propagation across mass interfaces is another example in which effects arise as a direct consequence of the discreteness of the medium, as gaps between beads in the vicinity of the interface are crucial for understanding the wave dynamics [2, 6]. These phenomena cannot be captured by the analytical approaches used to describe granular crystals developed so far, due to the assumption of a continuous medium used in such analytical approaches. Consequently, the study of wave propagation across interfaces is limited to numerical simulations.

Granular media have received a lot of attention from material scientists due to their application in the design of impact attenuating materials [18–23]. In order to properly make use of the shock absorbing capabilities of granular crystals, understanding the propagation of solitary waves is indispensable. In granular crystals, designing an impact attenuating material is equivalent to designing a medium that disintegrates or re-directs solitary waves in such a way that the impact of the wave on the area which is to be protected is mitigated. In 1D, so-called *granular containers* make use of the propagation of waves across mass interfaces in the design of a composite material that is capable of delaying and mitigating the impact of an incoming solitary wave. The simplest form of a granular container is a medium with lighter beads embedded in a medium with heavier beads [4, 6, 24]. At the first interface a solitary wave disintegrates and forms a multipulse structure inside the container, whereas at the second interface each of these pulses is partially transmitted and reflected. This leads to only a fraction of the initial pulse energy being transmitted after the pulse meets the two interfaces. The remaining energy is held back in the container in the form of several solitary waves which are reflected back forth, losing part of their energy in transmission at each reflection. Thus the impact of the initial solitary wave is attenuated by splitting it into many smaller waves which hit the end of the chain one after the other [6]. This principle of combining interfaces to manipulate the wave propagation can be further extended to more complex granular container structures [4].

Tapered chains are chains with slowly increasing bead masses; i.e. instead of having one interface with a relatively high difference in bead masses, tapered chains can be seen as a sequence of interfaces. This set-up reflects a fraction of the wave energy at each interface. Tapered chains are characterised by the tapering parameter $q \in (0, 1)$ that relates the radii R_i and R_{i+1} of two successive spherical beads in the tapered part of the chain by $R_{i+1} = (1 - q)R_i$. In numerical simulations it was

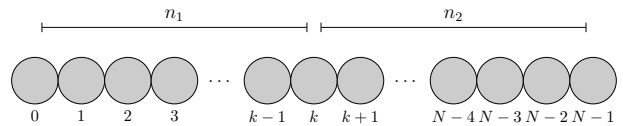


Figure 2: Granular chain composed of two media with interaction potential exponents n_1 and n_2 with the interface being at node k . The exponent difference is defined as $\Delta n = n_2 - n_1$. Note that in the experimental implementation the beads are not spherical in general.

observed that the wave attenuation is increased with increasing tapering q . The attenuation can be further enhanced in so-called *decorated tapered chains*, where every other bead in the decorated part of the chain is kept at the initial bead size [4, 25].

The propagation of solitary waves in granular chains across interfaces between media with different bead masses has been studied extensively [4]. Effects including reflection, transmission and emerging multipulse structures have been found and used to design composite materials for manipulating the propagation behaviour of incoming solitary waves [5, 6, 17, 26, 27].

In this paper we present a new way of creating interfaces between two types of granular crystals that offers an alternative method of affecting solitary wave propagation in composite media. Knowing that differences in bead masses can induce complex dynamics at interfaces, we want to investigate how abrupt changes in the interaction potential influence the wave propagation. While there are some results for interfaces between linear and nonlinear media [4], we are not aware of any work on interfaces between media with different nonlinearities. Therefore, we study the propagation properties for solitary waves travelling across interfaces between media with different interaction exponents n . For a schematic, see Fig. 2.

The underlying physical property causing the interface effects for mass interfaces is the inertia of the beads, i.e. the resistance to acceleration, for which the bead mass is a measure. These differences in acceleration behaviour lead to a disruption of the compression wave propagation causing the opening and closing of gaps and compression imbalances in the vicinity of the interface. The parameter n governs the shape of the interaction potential and thereby the shape of the interparticle force. And since according to Newton’s second law of motion the force is proportional to the acceleration of the particles we expect imbalances in the acceleration behaviour of the beads at the interface. Therefore, disruptions of the solitary wave propagation are expected in this case as well. Similarly to mass interfaces, the interface effects for different interaction exponents depend on whether the exponent increases or decreases along the propagation direction. We characterise interfaces by the difference $\Delta n = n_2 - n_1$ between the exponents in the two media.

II. INCREASING INTERACTION EXPONENT ALONG PROPAGATION DIRECTION

In order to induce waves in the granular chain the initial conditions of the beads are set as

$$u_1, \dots, u_N = 0, \quad v_1 = v^{(0)}, \quad \text{and} \quad v_2, \dots, v_N = 0, \quad (8)$$

where $v_k = \frac{du_k}{dt}$. This corresponds to the first bead hitting the granular chain from the left and thereby exciting beads in the system, resulting in wave propagation.

The beads are assumed to be made of stainless steel and dimensions are as used in the experimental set-up by Coste et al. in [10]. Furthermore, it is assumed that the distance between the two contact points of the beads is equal to the bead diameter used in [10]. The relevant physical parameters are shown in Table I.

Symbol	Property	Value
R	bead radius	4mm
Y	Young's modulus	$2.26 \times 10^{11} \text{Nm}^{-2}$
σ	Poisson's ratio	0.3
ρ	density	7650kgm^{-3}
m	mass	2.05g

Table I: Physical parameters used in simulations [10].

The initial conditions (8) are chosen such that the wave speed of the induced solitary wave is in the range of wave speeds experimentally tested in [10]. In computer units, i.e. after re-scaling, for spherical beads with masses as in Table I we set the initial velocity of the left striking bead to be $v^{(0)} = 1 \times 10^7$.

The value the initial velocity takes in computer units changes for different re-scaling factors; however in SI units the initial velocities are the same: approximately 0.11ms^{-2} . This initial velocity induces waves with wave speeds that are of the order of waves experimentally measured by Coste et al. [10].

The interaction potential exponent n can be changed experimentally by altering the contact geometry between the beads. However, changing the contact geometry will generally affect the prefactors a as well [3, 9]. For the sake of simplicity, it is assumed that the prefactors are constant over the entire range of exponents tested here. We set the value of the prefactors to the value for spherical beads as in Equations (3) and (4).

For typical experimental parameters of the chain [10], the factors scaling like na/m in front of the interaction term in the equation of motion are $\mathcal{O}(10^{12} \text{s}^{-2})$ in SI units, since

$$a = \mathcal{O}(10^9 \text{kg s}^{-2}), \quad m = \mathcal{O}(10^{-3} \text{kg}), \quad n = \mathcal{O}(1). \quad (9)$$

In order to scale this factor to $\mathcal{O}(1)$ we re-scale time by

$$t = \beta \tilde{t}, \quad \beta = \sqrt{\frac{m_0}{\mu n_0}}, \quad (10)$$

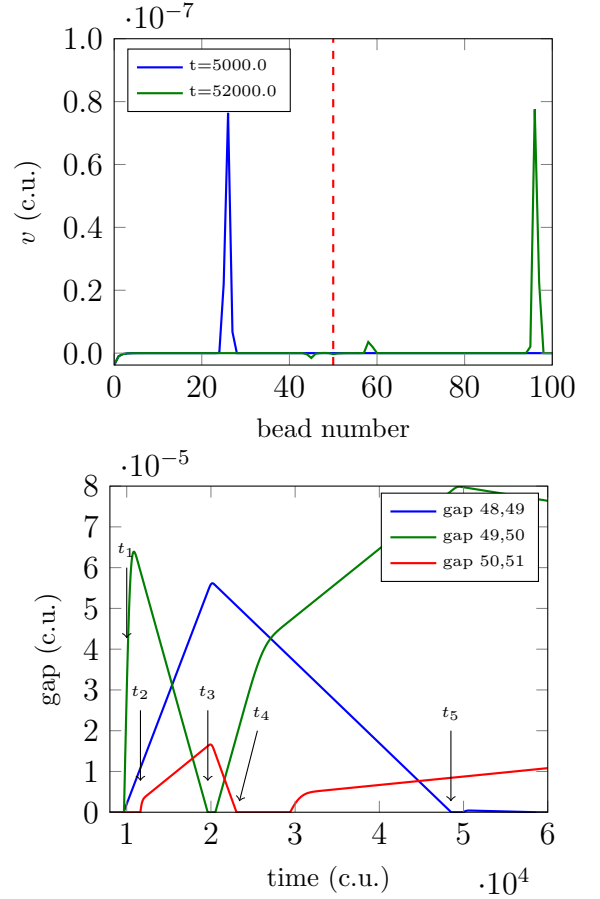


Figure 3: Solitary wave propagation across an interface between media with $n_1 = 3.0$ and $n_2 = 3.5$: waves before and after hitting the interface (top) and gaps emerging in the vicinity of the interface (bottom). In the top panel, the interface is indicated by the dashed red line.

where μ is the order of magnitude of a such that $\tilde{a} = a/\mu = \mathcal{O}(1 \text{kg s}^{-2})$, and m_0 and n_0 are typical values for the bead mass and interaction potential exponent respectively. Then the equation of motion after rescaling becomes

$$\begin{aligned} \frac{d^2 u_i(\tilde{t})}{d\tilde{t}^2} &= \frac{\beta^2}{m_i} W_i \\ &+ \frac{\beta^2 \mu n_{i-1,i}}{m_i} \tilde{a}_{i-1,i} (\Delta_{i-1,i} + u_{i-1}(\tilde{t}) - u_i(\tilde{t}))_+^{n_{i-1,i}-1} \\ &- \frac{\beta^2 \mu n_{i,i+1}}{m_i} \tilde{a}_{i,i+1} (\Delta_{i,i+1} + u_i(\tilde{t}) - u_{i+1}(\tilde{t}))_+^{n_{i,i+1}-1}. \end{aligned} \quad (11)$$

Details of the numerical approach and error analysis are provided in Appendix A.

Fig. 3 shows the bead velocities before and after the solitary wave hits an interface with $n_1 = 3.0$ and $n_2 = 3.5$. For interfaces with $\Delta n > 0$ we observe that

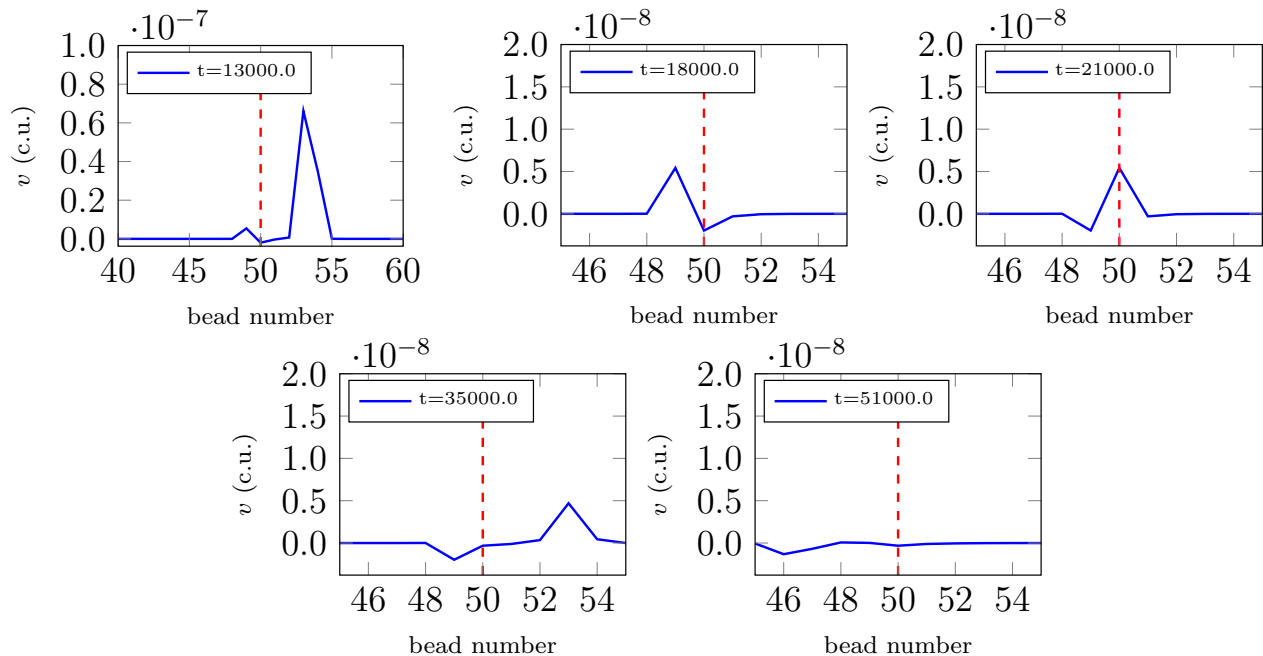


Figure 4: Solitary wave propagation across an interface between media with $n_1 = 3.0$ and $n_2 = 3.5$ for different times. The interface is indicated by the dashed red line.

most of the energy is transmitted to the medium on the right-hand side; however, there is one additional transmitted pulse and one reflected pulse, both about an order of magnitude smaller in peak velocity. A noteworthy behaviour is that the bead velocities in the vicinity of the interface freeze in a few configurations before all the energy is propagated away from the interface.

Whereas the arriving wave in the medium on the left immediately induces a wave of similar amplitude in the medium on the right, the two secondary pulses are delayed, i.e. they do not propagate away from the interface directly after the initial solitary wave hits it, but they freeze close to the interface for some time. This is due to the time it takes to close gaps between beads close to the interface that emerge upon the solitary wave hitting the interface, as shown in Fig. 3.

After the initial wave hits the interface at time t_1 , indicated in Fig. 4, the emerging gaps lead to bead 49 freely travelling forward while bead 50 is travelling backwards. The beads at the interface are frozen in this state between times t_2 and t_3 , when beads 49 and 50 exchange momenta in an elastic two-body collision. This new state is again frozen until time t_4 , when bead 50 closes the gap to its right neighbour and induces the secondary transmitted wave. The reflected wave starts propagating away from the interface at time t_5 when bead 49 reaches its left neighbour. Similar delays have previously been reported for granular containers with mass interfaces [6].

Bead 50 travelling backwards and thereby inducing the small reflected wave is essentially an instance of chain fragmentation in the the right-hand side medium. When

the initial solitary wave hits the interface at time t_1 a gap between bead 49 and bead 50 opens, and therefore the two media are disconnected. Bead 50 acts as a striker that hits the right medium inducing a solitary wave and chain fragmentation with some beads rebounding in the other direction.

Since the opening and closing of gaps is essential for the explanation of the secondary waves that emerge for interfaces with $\Delta n > 0$, we do not expect them to be captured by any continuum model, as gaps are a feature of the discreteness of granular crystals.

III. DECREASING INTERACTION EXPONENT ALONG PROPAGATION DIRECTION

For a wave propagating across an interface with $\Delta n < 0$ the effects are quite different. Fig. 5 shows the bead velocities before and after the initial solitary wave hits the interface for $n_1 = 3.0$ and $n_2 = 2.5$. There is a significant reflection and transmission, with the transmitted energy being converted into a multipulse structure. Unlike in the case discussed above, there is no delay of transmitted or reflected part of the wave. At the moment when the reflected wave starts to propagate away from the interface, the transmitted energy forms a pulse with a nearly rectangular shape. In the case shown here this means the first 8–9 beads behind the interface have roughly the same velocity. This nearly rectangular pulse splits and goes on to form the transmitted multipulse structure.

In previous numerical simulations it was observed that

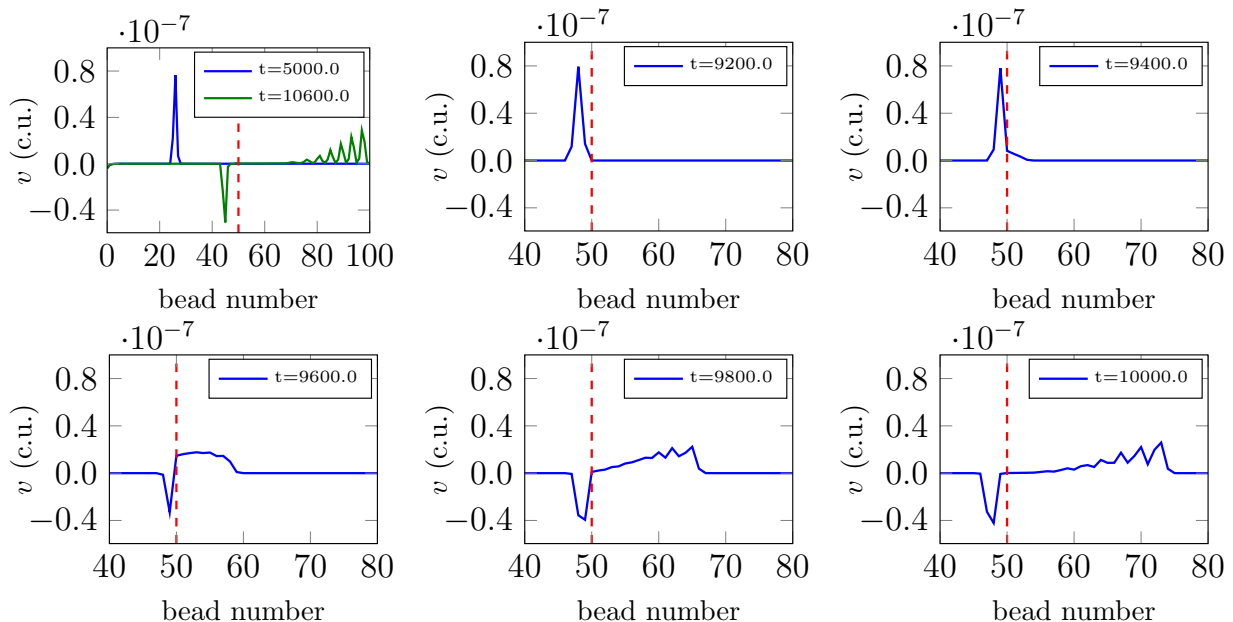


Figure 5: Solitary wave propagation across an interface between media with $n_1 = 3.0$ and $n_2 = 2.5$.

for rectangular initial conditions, i.e. the first l particles having the same initial speed, a multipulse structure with l waves emerges [2, 28]. The transmitted pulse in Fig. 5 resembles such initial conditions.

The reflected energy propagates away from the interface in the form of a single solitary wave, whose energy can be measured easily. We determine the range of beads that form the solitary wave by finding the beads with more than 0.1% of the peak bead velocity in the wave. As the energy carried by the wave is not purely kinetic, we also need to consider the potential energy stored in the interaction between the beads. Then for a solitary wave which is made up of s beads starting at the k^{th} bead, the wave energy is given by

$$E = \sum_{i=k}^{k+s} m_i v_i^2 + \sum_{j=k}^{k+s-1} a \delta_{j,j+1}^{n_1}, \quad (12)$$

where the first and second sum are the kinetic and potential energy carried by the wave respectively. The fraction of reflected energy $E_{\text{refl}}/E_{\text{in}}$, where E_{refl} and E_{in} are the reflected and initial energy, is shown in Fig. 6 as a function of n_1 and n_2 .

For $\Delta n < 0$, i.e. when significant reflection occurs, the contours in Fig. 6 are linear and collapse around the point $(n_1, n_2) \approx (1.65, 1.65)$, which is outside the plotted domain. Therefore, the reflected energy can approximately be described in terms of a new variable

$$\zeta = \frac{n_1 - 1.65}{n_2 - 1.65}, \quad (13)$$

as shown in Fig. 7.

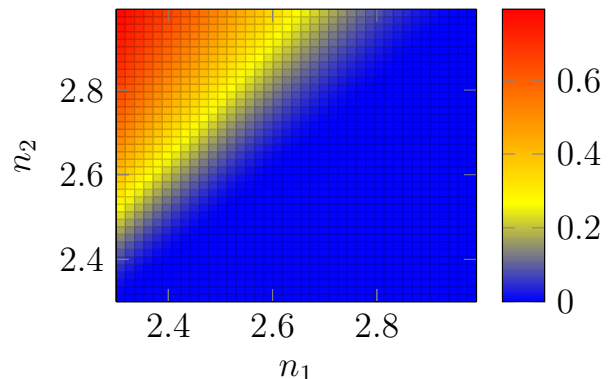


Figure 6: Reflected energy as function of n_1 and n_2 .

IV. TWO-PARTICLE VERSUS FEW-PARTICLE INTERACTIONS

Let us consider an interface between media with different bead masses as discussed in [4–6, 26], more specifically the case where a solitary wave is propagating from the lighter to the heavier medium. For large values of n most of the kinetic energy of a propagating solitary wave is carried by a single bead. In this case we can approximate the dynamics to be completely described by at most two particles interacting with each other at a given point in time, as the velocities of all other particles are essentially zero.

Under these assumptions, the effects arising from wave propagation across the interface can be derived from the interaction between the last particle with the lighter mass

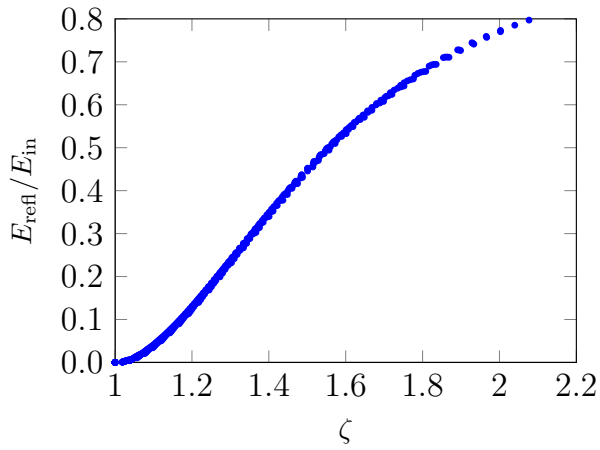


Figure 7: Simulated reflected energy as a function of the new variable ζ .

m at site k , and the first particle with the heavier mass M at site $k + 1$ [26]. For such a simple two-body collision, the velocities after the collision, v'_k and v'_{k+1} , are completely determined by the conservation of momentum and energy without having to consider the details of the interaction potential: $v'_k = \frac{m-M}{m+M}v_k$, $v'_{k+1} = \frac{2m}{m+M}v_k$, where v_k is the velocity of bead k before the collision and bead $k + 1$ is assumed to be initially at rest. Note that we need to assume the inter-particle force is repulsive and conservative, i.e. the collision is elastic and no energy is lost. As we have $m < M$, bead k moves in the opposite direction causing the reflected wave, whereas bead $k + 1$ moves to the right initialising the transmitted wave. A similar two-body argument can be given for the effects arising for a solitary wave propagating in the opposite direction [26].

Returning back to our case of interfaces between regions with different interaction potential exponents n , we can consider the interactions under the same two-body approximation. However, as mentioned above, the details of the interaction are irrelevant for the outcome of a two body collision and since the bead masses are equal we get $v'_k = 0 = v_{k+1}$, $v'_{k+1} = v_k$, i.e. the two particles simply exchange momenta. Therefore, in contrast to the mass interfaces, here the reduction to a two-body problem cannot explain any of the observed interface effects. Therefore, all of the observed phenomena must be fundamentally connected to few-body interactions.

This can also be elucidated by recalling that the interface here is constituted by a bead with different interaction potentials on its left and right side, rather than the boundary between two beads, as is true for mass interfaces. Therefore, we need at least three beads to interact in order for the different interaction potentials to play a role in the wave propagation.

At interfaces with $\Delta n < 0$, the number of particles interacting at the interfaces is significantly larger than

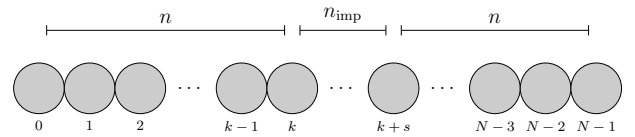


Figure 8: Granular chain with interaction exponent n with an impurity of s neighbour interactions with exponent n_{imp} .

three. We can define the number of particles that interact at the interface as the number of excited particles just before the reflected and transmitted waves part. We observe that at the interface the first couple of beads in the right medium are collectively excited by the collision with the incoming solitary wave, as shown in Fig. 5. In the collision process these collectively excited beads in the right-hand side medium can be imagined as forming a quasi-particle with a mass equal to the sum of its constituent bead masses. The incoming wave accelerates several particles in the right medium simultaneously and is then reflected off this quasi-particle, due to its heavier mass.

The number of particles involved in the interaction at the interface might also be the explanation for the decrease in reflected energy when n is increased uniformly on both sides. For larger n , the wavelength and therefore the number of particles involved in the formation of quasi-particles are smaller, which thereby could decrease the reflection.

V. CHAINS WITH IMPURITIES

Knowing that the abrupt changes in the interaction exponent between two media can cause complex wave propagation phenomena, one might ask what happens when there is a change in the interaction exponent in a localised region within an otherwise monodisperse chain. We consider the situation depicted in Fig. 8, in which the force between s consecutive bead-bead pairs within the chain is governed by the interaction exponent n_{imp} which are embedded in a chain with interaction exponent n . In this set-up, $s + 1$ beads have at least one interaction with a neighbouring bead with the exponent n_{imp} . In order to distinguish impurities from interfaces, we denote the difference in the exponent between the medium and the impurity as $\delta n = n_{\text{imp}} - n$.

Fig. 9 shows two examples of granular crystals with impurities for $\delta n > 0$ and $\delta n < 0$. Upon hitting the impurity, the initial solitary wave is partially reflected with the remaining energy being converted into a multipulse structure. In contrast to interfaces, here we obtain similar qualitative behaviour independently of the sign of δn .

An interesting observation we make is that for large negative δn , the impurity beads behave collectively, i.e. their velocities are identical. Fig. 10 shows two exam-

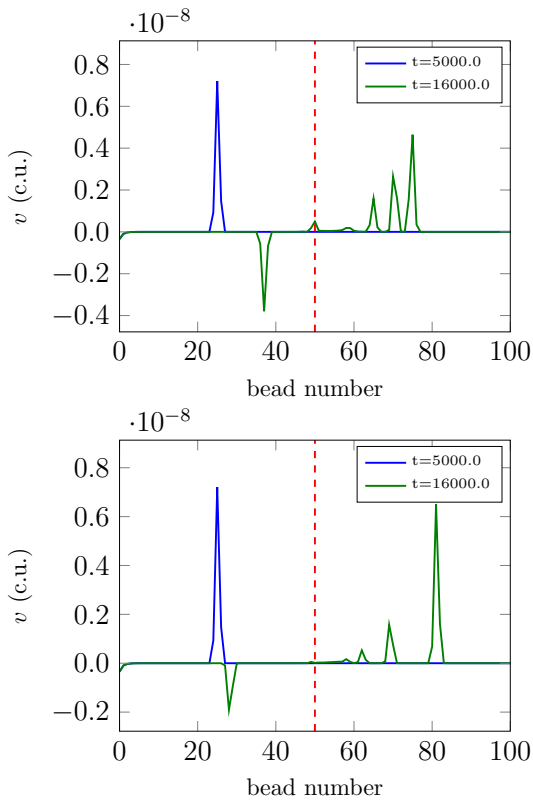


Figure 9: Granular crystals with impurities with $s = 1$, $n = 3.0$ for $n_{\text{imp}} = 3.5$ (top) and $n_{\text{imp}} = 2.5$ (bottom). The red dashed line indicates bead k (c.f. Fig. 8).

ples for the impurity bead velocities during the interaction with the incoming solitary wave for $s = 1$. Whereas for $\delta n = -0.25$ there is an asymmetry between the two impurity beads, they are completely synchronised for $\delta n = -1.5$. This clearly shows quasi-particle behaviour in which the two impurity beads act as one particle of mass $2m$, similar to the observations for interfaces.

We can compare the collision of the solitary wave with the impurity to the two-body approximation as discussed in Section IV. Fig. 11 shows the ratio of the peak bead velocities between reflected and incoming solitary wave $|v_{\text{out}}/v_{\text{in}}|$ for different values of n and s . For large interaction exponent differences between the medium and the impurity, the reflected velocity converges to the velocity one would get from a particle with mass m colliding with a particle of mass $(s + 1)m$ at rest. Therefore the process of the solitary wave interacting with an impurity is described well by the quasi-particle explanation. For small values of n the reflected velocity does not quite reach the value predicted by the two-body approximation. This is due to the fact that the incoming wave has a larger wavelength, hence approximating it by the motion of a single bead is inaccurate.

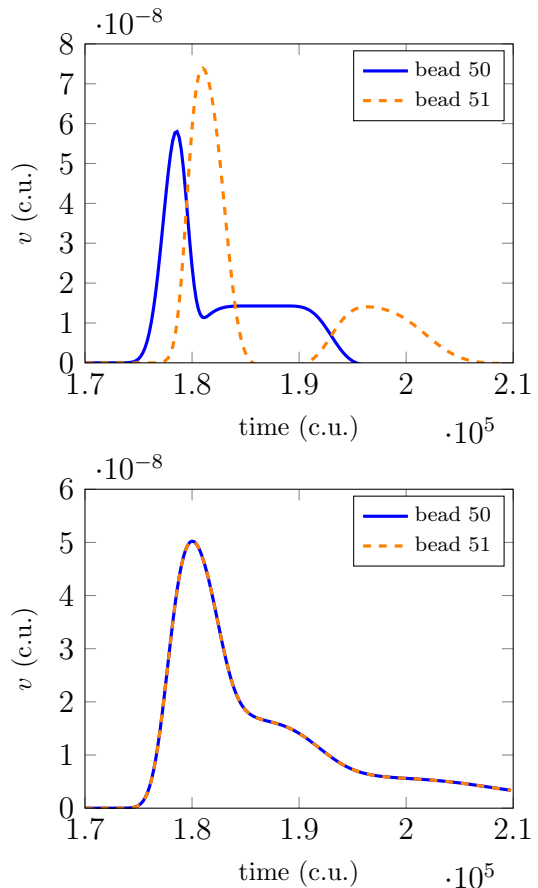


Figure 10: Impurity bead velocities with $n = 4.0$ and $s = 1$ for $\delta n = -0.25$ (top) and $\delta n = -1.5$ (bottom). The two lines are not distinguishable in the bottom panel.

VI. STABILITY UNDER SYSTEM PERTURBATIONS

The analysis of the dynamics of the beads in the vicinity of the interface shows that the numerically observed phenomena depend on the timing of gaps opening and closing and on the shape of the initially transmitted pulse. In experimental set-ups, the conditions might not be as well-controlled as in the numerical simulation due to the finite precision of the experimental apparatus. In order to investigate the stability of the previously observed effects under small perturbations of the chain parameters, the interaction potential exponent is randomly perturbed by

$$n_i^{\text{pert}} = n_i + n_i^{\text{rand}}, \quad i \in \{0, \dots, N - 2\}, \quad (14)$$

where n_i is the initial exponent and n_i^{rand} is taken from a Gaussian distribution with standard deviation σ and mean 0. However, the additional constraint $n_i^{\text{pert}} > 2.0$ is imposed in order to stay in the non-linear regime. The

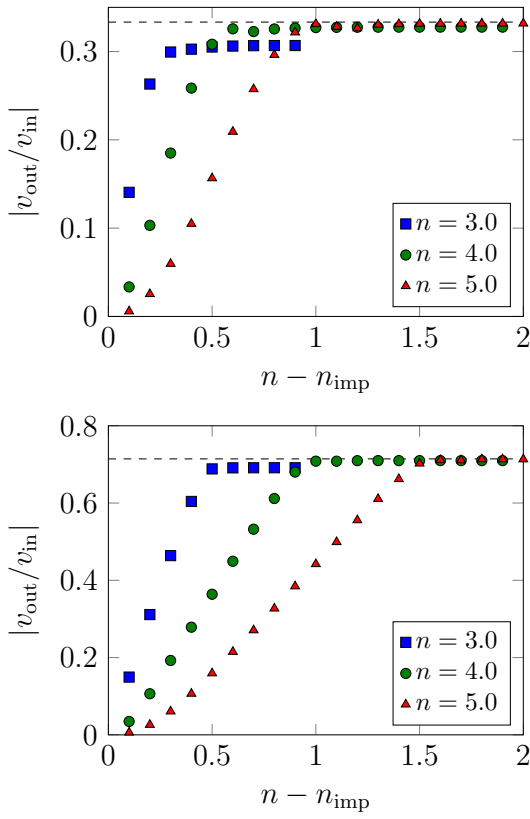


Figure 11: Ratio of the peak bead velocities between reflected and incoming solitary wave for impurities with different numbers of impurities s : $s = 1$ (top) or $s = 5$ (bottom). The dashed line indicates the velocity of a bead with mass m scattering of a bead with mass $(s + 1)m$.

interaction exponent difference $\Delta n = n_2 - n_1$ provides a scale to which the introduced randomness can be compared.

Fig. 12 shows the effect of the perturbation for the propagation of a solitary wave across an interface with $\Delta n > 0$. The first observation is that by introducing the perturbation, smaller waves behind the solitary wave develop, even in the monodisperse part of the chain. These smaller waves interfere with the two delayed secondary waves propagating away from the interface. However, a similar qualitative behaviour of the delayed secondary waves is observed up to the point where the smaller waves arising from the perturbations are of comparable size. Secondly, the gaps arising near the interface, which are responsible for the delayed transmitted and reflected secondary pulses, close faster due to interactions with waves arising from the impurities.

The effects of perturbation (14) on the propagation across an interface with $\Delta n < 0$ are shown in Fig. 13. We observe that the initial rectangular pulse, which causes the transmitted multipulse structure, develops for all tested perturbation strengths. Again, the agreement

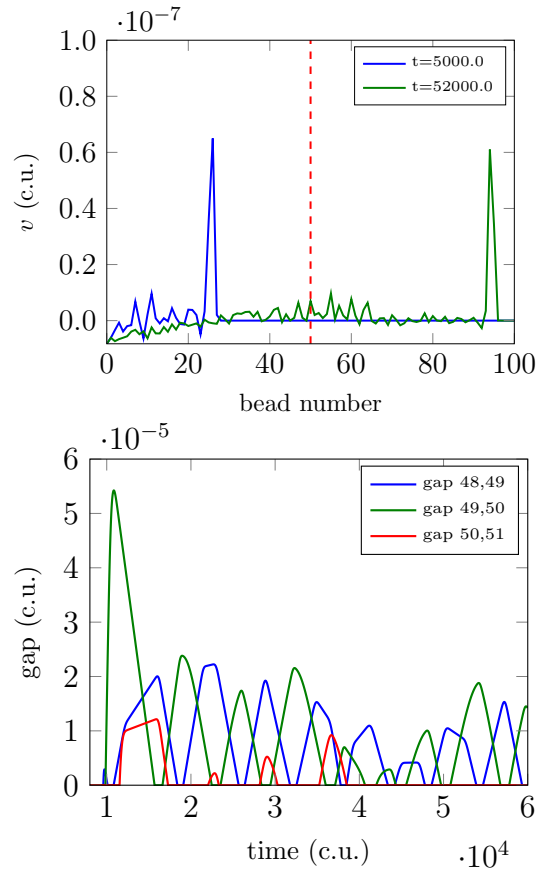


Figure 12: Effect of perturbation (14) for an interface with $\Delta n > 0$, given $\sigma/\Delta n = 0.05$.

with the unperturbed case is determined by the relative sizes of smaller waves induced by the perturbations and the features arising from the interface, such that the leading peaks of the multipulse structure are clearly visible even for relatively large perturbations whereas the smaller tail is lost in the noise.

For $\Delta n > 0$ the observed interface phenomena are present for perturbations of up to 1% of the interaction potential difference Δn , whereas the multipulse structure and wave reflection for $\Delta n < 0$ are present for perturbations of more than 5%. Therefore, we anticipate that the effects at interfaces between different interaction potentials would be obtainable experimentally for both $\Delta n > 0$ and $\Delta n < 0$.

VII. COMBINATION OF MASS AND INTERACTION EXPONENT INTERFACES

Now that we know about the effects of both mass and interaction exponent interfaces, we can study how the combination of both types of interfaces influences the solitary wave propagation (for a schematic, see Fig. 14). In order to keep the parameter space manageable, we fix

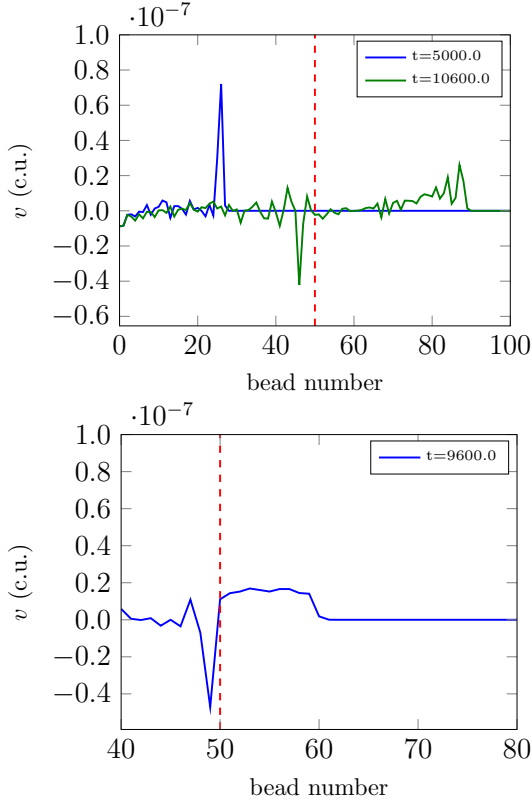


Figure 13: Effect of perturbation (14) with $\sigma/\Delta n = 0.05$ on solitary wave propagation across an interface between media with $n_1 = 3.5$ and $n_2 = 3.0$: waves before and after hitting the interface (top) and collective excitation of the beads in the right medium (bottom). The interface is indicated by the dashed red line.

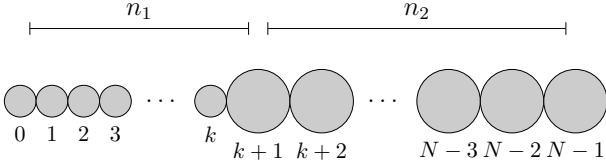


Figure 14: Combined mass and interaction exponent interface. Note that the mass on the right-hand side can also be smaller than on the left.

the parameters of the left medium to $n_1 = 3.0$ and bead mass $m_1 = m$ as used in the previous simulations, and only change the parameters for the right medium. We vary Δn in $[-0.5, 0.5]$ and the ratio m_2/m_1 between the bead mass on the left and on the right in $[1/8, 8]$.

Fig. 15 shows the reflected energy as a function of the two interface parameters. Note that for visualisation purposes where no reflection was detected the value for the reflected energy was set to the minimum value detected over the entire parameter range. Therefore, for the entire

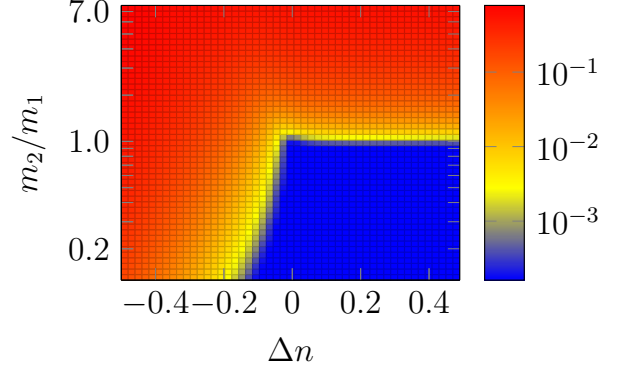


Figure 15: Reflected energy as function of Δn and m_2/m_1 .

dark blue area in the plot, no significant reflection could be detected.

In the bottom-right part of Fig. 15 there is no reflection; this is what we would expect from what we know of both types of interfaces in this parameter regime. Similarly, for the parameters in the top left corner both types of interfaces separately show reflection, which is also the case for the combined interface. In the top-right corner, i.e. for $\Delta n > 0$ and $m_2/m_1 > 1$, the reflection is mainly determined by the mass difference with significant reflection for all $m_2/m_1 > 1$. This seems plausible as the difference in interaction exponents for $\Delta n > 0$ had only small effects on the wave propagation.

However, for $\Delta n < 0$ and $m_2/m_1 < 1$, we arrive at contradicting predictions using our knowledge from the separate study of these two types of interfaces: for mass interfaces we expect a full disintegration of the wave without any reflection, but for interaction exponent interfaces we would predict the emergence of a multipulse structure with significant reflection. For the combined interface we observe a transition between regions with and without reflection. The contour at which the transition occurs can be interpreted in the framework of the quasi-particle explanation: it is the set of parameters where the effective mass of the quasi-particle on the right-hand side and the bead mass on the left-hand side are equal. In other words, the mass difference in the quasi-particle collision is balanced out by the difference of the bead masses m_1 and m_2 .

VIII. CONCLUSIONS

We have investigated interfaces between distinct Hertz-like granular crystals with different interaction exponents n_1 and n_2 . For $\Delta n > 0$, we obtain mainly transmission of the incoming wave with one transmitted and one reflected secondary wave forming at the interface with a time delay to the primary transmitted wave. The secondary waves are around one order of magnitude smaller in peak bead

velocity than the original wave and their formation involves the opening and closing of gaps in the vicinity of the interface. The emergence of these secondary waves is thus a direct consequence of the discreteness of the granular chain. This effect is not expected to be captured by any models using the continuum approximation.

For interfaces with $\Delta n < 0$, both transmission and reflection of the solitary wave occur. Whereas the reflected part of the initial energy propagates away from the interface in form of a single solitary wave, the transmitted energy is converted into a multipulse structure. Combining both mass and interaction exponent interfaces we could find a transition between parameter regimes with and without reflection of the solitary wave. This is in accordance with our explanation for reflection in the absence of bead mass differences for the case of pure interaction exponent interfaces.

Although similarities between the effects at mass and interaction exponent interfaces exist, the underlying dynamics at the vicinity of the interface are fundamentally different. Whereas mass interfaces can be explained in terms of collisions between single beads with different masses, the phenomena at interaction exponent interfaces with $\Delta n < 0$ involve few-body dynamics close to the interface. Moreover, we found that the first few beads on the right-hand side of the interface are collectively accelerated causing the partial reflection of the incoming wave. We were able to give a simple interpretation of the process in terms of a quasi-particle collision.

One extension of this work might be the study of interfaces involving different types of interaction potentials. In this paper, we have considered interactions that are purely based on contact forces, which lead to Hertz-like power-law potentials. However, one could imagine having additional or different types of interactions between the particles. We are aware of one study using an external magnetic dipole field to introduce additional forces between the beads due to magnetisation. The additional interaction introduces dispersion, which in turn leads to wave attenuation [29]. These different types of interactions could be used to create interfaces which yield interesting wave propagation dynamics.

Another logical step in the study of interfaces between granular crystals with different interaction exponents under contact forces is the generalisation to higher dimensions. In higher dimensions the packing of the beads and the direction of the compression wave with respect to the main axes of the granular crystal influence the propagation in monodisperse media [30]. When interfaces are present, higher dimensions offer additional degrees of freedom for the wave propagation, namely the angle at which the wave meets the interface. In 2D a law for the refraction and reflection of solitary waves at mass interfaces similar to Snell's law in optics was found [31]. As we have shown, in 1D there are similarities between the effects arising when solitary waves are propagation across mass and interaction exponent interfaces. Therefore, in 2D there could be similar refraction and transmission ef-

fects for interaction exponent interfaces.

Appendix A: Numerical Approach

For a given chain with N beads Equation (7) constitutes a coupled set of N second order non-linear ODEs. Defining the vector of bead displacements as

$$\vec{u} = \begin{bmatrix} u_1 \\ u_2 \\ \vdots \\ u_N \end{bmatrix}, \quad (\text{A1})$$

we can formally write the equation of motion (7) as

$$\ddot{\vec{u}} = \vec{f}(\vec{u}), \quad (\text{A2})$$

where $\ddot{\vec{u}}$ denotes the second time derivative of \vec{u} . By defining the combined vector of bead displacements and velocities

$$\vec{z} = \begin{bmatrix} u_1 \\ \vdots \\ u_N \\ v_1 \\ \vdots \\ v_N \end{bmatrix} = \begin{bmatrix} \vec{u} \\ \vec{v} \end{bmatrix} \quad \text{where} \quad \vec{v} = \begin{bmatrix} v_1 \\ \vdots \\ v_N \end{bmatrix} = \dot{\vec{u}}, \quad (\text{A3})$$

Equation (A2) can be converted into a system of $2N$ first order non-linear ODEs that can be written as

$$\dot{\vec{z}} = \vec{F}(\vec{z}) = \begin{bmatrix} \vec{v} \\ \vec{f}(\vec{u}) \end{bmatrix}. \quad (\text{A4})$$

The main computational step for simulating the dynamics in granular crystals is solving Equation (A4), for N of order 10^2 to 10^3 .

All of the code written for carrying out the simulations and data analysis is written in Python [32], where we mostly use arrays from the Python extension NumPy [33] for data storage. Where applicable, we use the scientific computing library SciPy [34] which has implemented functionality similar to MATLAB.

As mentioned above, the equation of motion for the particles at the boundaries has only one interaction term since it has only one neighbour. In order to avoid having to use separate equations for the boundaries or looping through particles in the ODE solver, we added two ghost particles at the ends of the chain with the interaction prefactor a to the first real particle being zero. Therefore the state vector \vec{z} in the simulation becomes

$$\vec{z}_{\text{sim}} = \begin{bmatrix} 0 \\ \vec{u} \\ 0 \\ \vec{v} \end{bmatrix}, \quad (\text{A5})$$

where there are no extra entries for the velocity of the ghost particle, since they do not move. This way we can write the first order ODE (A4) solely in terms of Numpy-array objects.

For solving the ODE system (A4) we use a solver provided by the built-in ODE interface *scipy.integrate.ode* [35] in the SciPy library. We use the variable-coefficient ODE solver VODE [36–38], which in turn uses Adams-Moulten and backward differentiation methods depending on the stiffness of the system.

As there are no analytical solutions of the full discrete ODE system (A4), there is no direct way to determine the correctness and accuracy of our numerical scheme used for our simulations. However, we can make use of both previous results and expected physical properties of the system to evaluate the numerical accuracy. Simulations of wave propagation across mass interfaces are produced by our numerical scheme and can be used to correctly emulate the behaviour in the original publication [5]. Similarly our simulations show good qualitative agreement with results in the literature in the case of randomised bead masses and solitary wave collisions [4, 14].

In order to evaluate the accuracy quantitatively we can make use of the energy conservation in the chain. As there are no dissipative effects built in to the model used to describe the dynamics, we expect all bead-bead collisions to be fully elastic, i.e. conserve the total energy. Therefore the energy loss—or gain—qualifies as a measure of the accuracy of the simulation. We use the total kinetic energy

$$E^{\text{kin}} = \sum_{i=0}^{N-1} m_i v_i^2, \quad (\text{A6})$$

to determine how well the energy is conserved. We define the energy conservation error as

$$\text{error} = \left| \frac{E_{\text{start}}^{\text{kin}} - E_{\text{end}}^{\text{kin}}}{E_{\text{start}}^{\text{kin}}} \right|, \quad (\text{A7})$$

where $E_{\text{start}}^{\text{kin}}$ and $E_{\text{end}}^{\text{kin}}$ are the total kinetic energies in the chain at the start and the end of the simulation respectively.

Every granular crystal without externally applied forces reaches a steady-state of the bead velocities for long enough simulation times, i.e. the beads move at constant velocity with every bead having a smaller velocity than its right-hand-side neighbour. In terms of bead velocities the steady state translates to the bead

velocities increasing monotonously with the bead number. Two subtleties need to be pointed out here: firstly, in order to have purely kinetic energy in the system we additionally need to require the bead overlap to be zero and secondly, for all practical purposes it is enough to require

$$v_{i+1} - v_i > -10^{-5} \times \max_{j \in \{0, \dots, N-1\}} |v_j|,$$

rather than actual monotonicity. This simplification reduces the simulation time needed to reach the steady state by orders of magnitude, while the additional errors introduced by it are negligible compared to the overall energy conservation error.

In such a situation the total energy in the chain is purely kinetic as the beads are drifting apart without touching each other. Therefore, we measure the kinetic energy at time $t = 0$, before the the striking bead 0 has any overlap with bead 1, and after the chain has reached the steady state. This justifies neglecting the potential energy for calculating the energy conservation error.

In the VODE solver the estimated local error \vec{e} is controlled by

$$\left| \frac{e_i}{\text{EWT}_i} \right| \lesssim 1, \quad i \in \{0, \dots, N-1\}, \quad (\text{A8})$$

for each component of the error, where the error weights are defined as

$$\text{EWT}_i = \text{rtol} \times |z_i| + \text{atol}, \quad (\text{A9})$$

where *rtol* and *atol* are the relative and absolute tolerances respectively [37, 38]. Actually we would have to consider the two ghost particles here as well. However, we will neglect them for simplicity as their position and velocity variables do not change and therefore do not introduce errors.

One can set *rtol* = 0 or *atol* = 0 to have a purely absolute tolerance or purely relative tolerance respectively. Fig. 16 shows the energy conservation error as a function of the two tolerances. We observe that by setting strict tolerances in the simulation the error shrinks to nearly machine precision. This shows that our numerical scheme indeed conserves energy as would be expected from the physical system. In the simulations presented here we choose the tolerances such that the energy conservation error is $\mathcal{O}(10^{-4})$ or smaller. This has shown to be a good trade-off between accuracy and runtime.

-
- [1] H. M. Jaeger, S. R. Nagel, and R. P. Behringer, *Rev. Mod. Phys.* **68**, 1259 (1996).
 - [2] V. F. Nesterenko, *Dynamics of heterogeneous materials* (Springer, New York, 2001).
 - [3] K. L. Johnson, *Contact mechanics* (Cambridge University Press, Cambridge, 1985).

- [4] S. Sen, J. Hong, J. Bang, E. Avalos, and R. Doney, *Physics Reports* **462**, 21 (2008).
- [5] L. Vergara, *Phys. Rev. Lett.* **95**, 108002 (2005).
- [6] L. Vergara, *Phys. Rev. E* **73**, 066623 (2006).

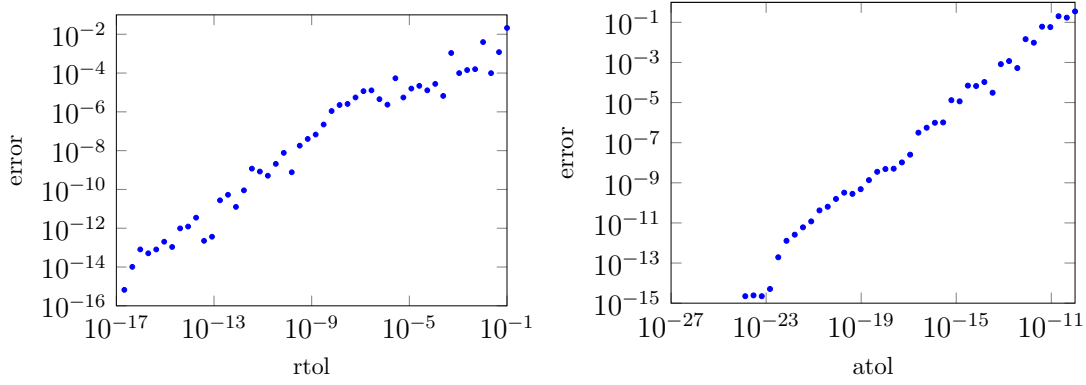


Figure 16: Energy conservation error as a function of the relative tolerance (left) and the absolute tolerance (right). For each plot the other tolerance was fixed at 0.0.

- [7] D. Khatri, D. Ngo, and C. Daraio, *Granular Matter* **14**, 63 (2012).
- [8] H. Hertz, *Journal für die reine und angewandte Mathematik* **92**, 156 (1882).
- [9] L. D. Landau, E. M. Lifšic, J. B. Sykes, and W. H. Reid, *Theory of elasticity* (Pergamon Press, Oxford, 1963).
- [10] C. Coste, E. Falcon, and S. Fauve, *Phys. Rev. E* **56**, 6104 (1997).
- [11] V. F. Nesterenko, *Journal of Applied Mechanics and Technical Physics* **24**, 733 (1983).
- [12] A. N. Lazaridi and V. F. Nesterenko, *Journal of Applied Mechanics and Technical Physics* **26**, 405 (1985).
- [13] E. Hascoët and H. J. Herrmann, *The European Physical Journal B - Condensed Matter and Complex Systems* **14**, 183 (2000).
- [14] M. Manciu, S. Sen, and A. J. Hurd, *Phys. Rev. E* **63**, 016614 (2000).
- [15] F. S. Manciu and S. Sen, *Phys. Rev. E* **66**, 016616 (2002).
- [16] J. Hong and A. Xu, *Applied Physics Letters* **81**, 4868 (2002).
- [17] V. F. Nesterenko, C. Daraio, E. B. Herbold, and S. Jin, *Phys. Rev. Lett.* **95**, 158702 (2005).
- [18] M. A. Porter, C. Daraio, I. Szelengowicz, E. B. Herbold, and P. Kevrekidis, *Physica D: Nonlinear Phenomena* **238**, 666 (2009).
- [19] W. P. Schonberg, H. A. Burgoyne, J. A. Newman, W. C. Jackson, and C. Daraio, *Procedia Engineering* **103**, 52 (2015).
- [20] G. Gantzounis, M. Serra-Garcia, K. Homma, J. M. Mendoza, and C. Daraio, *Journal of Applied Physics* **114**, 093514 (2013).
- [21] C. S. Chang and J. Gao, *International Journal of Non-Linear Mechanics* **30**, 111 (1995).
- [22] A. Leonard and C. Daraio, *Phys. Rev. Lett.* **108**, 214301 (2012).
- [23] N. W. Mueggenburg, H. M. Jaeger, and S. R. Nagel, *Phys. Rev. E* **66**, 031304 (2002).
- [24] J. Hong, *Phys. Rev. Lett.* **94**, 108001 (2005).
- [25] R. Doney and S. Sen, *Phys. Rev. Lett.* **97**, 155502 (2006).
- [26] M. Manciu, Ph.D. thesis, SUNY-Buffalo (2000).
- [27] C. Daraio, V. F. Nesterenko, E. B. Herbold, and S. Jin, *Phys. Rev. Lett.* **96**, 058002 (2006).
- [28] E. J. Hinch and S. Saint-Jean, *Proceedings of the Royal Society of London A: Mathematical, Physical and Engineering Sciences* **455**, 3201 (1999).
- [29] D. Leng, X. Wang, G. Liu, and L. Sun, *AIP Advances* **6**, 025321 (2016).
- [30] M. Manjunath, A. P. Awasthi, and P. H. Geubelle, *Granular Matter* **16**, 141 (2014).
- [31] A. M. Tichler, L. R. Gómez, N. Upadhyaya, X. Campman, V. F. Nesterenko, and V. Vitelli, *Phys. Rev. Lett.* **111**, 048001 (2013).
- [32] URL www.python.org.
- [33] URL <http://www.numpy.org>.
- [34] URL www.scipy.org.
- [35] *scipy.integrate.ode* (2008), URL <http://docs.scipy.org/doc/scipy/reference/generated/scipy.integrate.ode.html>.
- [36] P. N. Brown, G. D. Byrne, and A. C. Hindmarsh, *SIAM Journal on Scientific and Statistical Computing* **10**, 1038 (1989).
- [37] G. D. Byrne and A. C. Hindmarsh, *ACM Trans. Math. Softw.* **1**, 71 (1975).
- [38] P. N. Brown and A. C. Hindmarsh, *Vode source code*, URL <http://www.netlib.org/ode/vode.f>.